Model for a Brownian ratchet with improved characteristics for particle separation

Andrej Grimm,[1] Holger Stark,[2] and Johan R. C. van der Maarel[1]
[1]*Department of Physics, Biophysics and Complex Fluids Group, National University of Singapore, 2 Science Drive 3, Singapore 117542*
[2]*Institut für Theoretische Physik, Technische Universität Berlin, Hardenbergstrasse 36, D-10623 Berlin, Germany*
(Received 14 August 2008; revised manuscript received 22 April 2009; published 3 June 2009)

We introduce an extension of the simple on-off ratchet by including a second asymmetric sawtooth potential with half the periodicity and inverse asymmetry in the ratchet cycle. As a result of this additional potential, the Brownian particles exhibit reversal of the direction of their mean displacement when relevant parameters such as the on time of the potentials are varied. This direction reversal offers new opportunities for microfluidic particle separation in sieve devices. Based on the results of our extended ratchet model, we propose two designs. Compared to the classical microfluidic sieve, the proposed devices can be made of significantly smaller sizes without sacrificing the resolution of the separation process. In fact, one of our devices can be reduced to a single channel. We study our extended ratchet model by Brownian dynamics simulations and derive analytical and approximative expressions for the mean displacement using an extension of the method of discrete steps. We show that these expressions are valid in relevant regions of the parameter space and that they can be used to predict the occurrence of direction reversal.

DOI: 10.1103/PhysRevE.79.061102 PACS number(s): 05.40.−a, 82.45.−h, 05.10.−a

I. INTRODUCTION

The effective separation of micron-sized particles poses a challenge for integrated microfluidic devices [1,2]. A particularly promising strategy is the separation based on the rectification of Brownian motion caused by the ratchet effect. It has experimentally and theoretically been demonstrated that this strategy can be implemented with microfabricated sieve devices [3–6]. In such a sieve, the suspended particles are driven through rows of asymmetric obstacles with the help of an electric field. The ratchet induces a component of the flow in a direction parallel to the rows of obstacles. The net flow of particles through the device is, hence, inclined with respect to the electric field. Differences in the magnitude of the ratchet induced component of the flow between distinct types of particles lead to different inclinations and to particle separation. Due to the resolution in the direction of the flow, this separation process is also known as "vector chromatography" [7]. For pointlike particles the magnitude of the induced flow has been calculated by means of Brownian ratchet theory [5,6]. Finite-size effects have been studied by means of a network theory [8]. Compared to conventional technologies, such as gel electrophoresis, sieve devices offer some advantages including continuous separation. However, the classical implementation of the sieve device has two major drawbacks. First, the number of rows of obstacles, and consequently the size of the device, has to be increased in order to improve the resolution. Second, a localized injection of the particles is required for optimal separation. Localized injection, however, reduces the throughput of the device. It has been pointed out in Ref. [9] that the exploitation of the direction reversal effect would overcome both disadvantages.

Direction reversal refers to ratchets in which the direction of the induced flow can be inverted by the adjustment of certain system parameters [10]. If the direction of the induced flow also depends on the properties of the particles, a proper tuning of the system parameters can lead to opposite directions of the flows pertaining to distinct types of particles. Direction reversal has experimentally been observed for colloids in holographic optical trapping devices [11]. Most theoretical work on direction reversal has been done for ratchets with stochastically switching potential states [12–14]. These so-called fluctuating ratchets have the advantage that the induced flow can be calculated by standard methods. Fluctuating ratchets have implications in the field of biological molecular motors, but they are relatively irrelevant in the context of particle separation. Most experimental work on Brownian ratchets is based on potential states which are periodically changed [15–18]. To the best of our knowledge, direction reversal in the latter type of on-off ratchet has attracted little attention [19]. This might be a reason why the benefits of direction reversal have so far not been exploited for the design of separation devices. However there have been several contributions describing direction reversal in related fields, e.g., ratchets with non-Gaussian noise [20], ratchets with space and time-dependent modulation of the potential states [21], and direction reversal in combination with absolute negative mobilities [22–24].

The standard on-off ratchet relies on an asymmetric sawtooth potential that is turned on and off and thereby induces a drift in one direction. A simple modification of this ratchet replaces the sawtooth potential in every second on state by a sawtooth potential of inverse asymmetry and half the spatial periodicity. The second sawtooth potential alone would induce a drift in the reverse direction. We show that in such an extended ratchet the average drift direction can be controlled by variation in system parameters such as the time during which the potentials are switched on. The principle of our extended ratchet is simple and therefore attractive for constructing microfluidic sieves for particle separation. In particular, since the particles to be separated drift in opposite directions, the size of microfluidic sieves can be reduced to a single channel without sacrificing the resolution of the separation process. We propose two possible designs of the microfluidic devices. In the first design, every second row of the obstacles in the classical sieve is replaced by a row of obstacles with half the spatial periodicity and inverse asym-

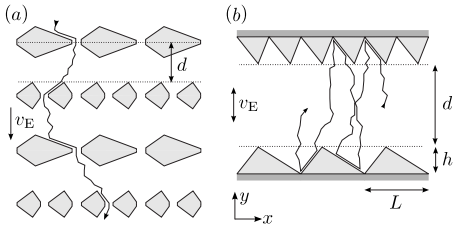

FIG. 1. Microfluidic devices for particle separation that benefit from the effect of direction reversal. (a) A microfluidic sieve device. The solid line represents an example trajectory of a particle driven by a constant electric field with electrophoretic velocity v_E. The gray objects refer to the obstacles. (b) As in panel (a) but for a microfluidic channel device. The particles are driven by a periodically inverted electric field back and forth across the channel.

metry [see panel (a) of Fig. 1]. The particles are driven through the device with the help of an externally applied electric field and they alternately interact with the two types of rows of obstacles. In the second proposed design, the sawtooth shaped obstacles line the opposing walls of a single channel. Here, the particles are driven back and forth between the walls with the help of a periodically inverted electric field [see panel (b) of Fig. 1]. In the paper, we first investigate the extended on-off ratchet in detail and then demonstrate how our results can be applied to the proposed microfluidic designs.

The paper is organized as follows. In Sec. II, we introduce the extended on-off ratchet model. We show that the model and its governing Langevin equation are described by four independent dimensionless parameters. With the help of Brownian dynamics simulations, we identify those parameters that are able to tune the direction of the induced particle flow. In Sec. III, analytical expressions for the mean displacement per ratchet cycle based on the method of discrete steps are presented. We first treat the extended on-off ratchet in the regime where the particles have enough time to drift into the potential minima. Then we extend the range of validity of the method of discrete steps to smaller on times by introducing what we call the split-off approximation. It is capable of reproducing our simulation results in relevant regimes of the parameter space. In Sec. IV, we explain how the performance of the proposed microfluidic devices can be described by the extended on-off ratchet. For this purpose, we map the parameters of the devices onto the characteristic parameters of the extended on-off ratchet. Finally, we validate our predictions with the help of Brownian dynamics simulations for the microfluidic channel device.

II. EXTENDED ON-OFF RATCHET

A. Details of the model

In a simple on-off ratchet a Brownian particle moves under the influence of a potential V_1, which is periodically switched on and off. A widely used potential is the asymmetric sawtooth potential. The form of the potential and the cycle of the simple ratchet are schematically depicted in panels (a) and (b) of Fig. 2, respectively. The potential V_1 is characterized by a spatial period L, asymmetry a, and amplitude $\hat{V}$. The asymmetry parameter a determines the shape of the potential and has a value in the range from zero to one. When the potential is switched off during a time t_{off}, the particle diffuses freely along the x axis. When the potential is switched on during a time t_{on}, besides diffusion the particle drifts coherently toward a minimum of the sawtooth potential. The interplay of the diffusion and the coherent drift rectifies the motion of the particle. Note that in this model the motion is always one dimensional along the x axis. The magnitude of the mean displacement for an ensemble of particles is determined by the properties of the potential as well as by the diffusional behavior of the particles. In contrast, the direction of the mean displacement is exclusively determined by the value of the asymmetry parameter a [25]. For $a<0.5$, the mean displacement is in the positive direction along the x axis, whereas for $a>0.5$ the particle will move on average in the negative direction. A simple on-off ratchet with asymmetry $(1-a)$ induces exactly the opposite mean displacement as a ratchet with asymmetry a. In the symmetric situation with $a=0.5$, no mean displacement will be observed.

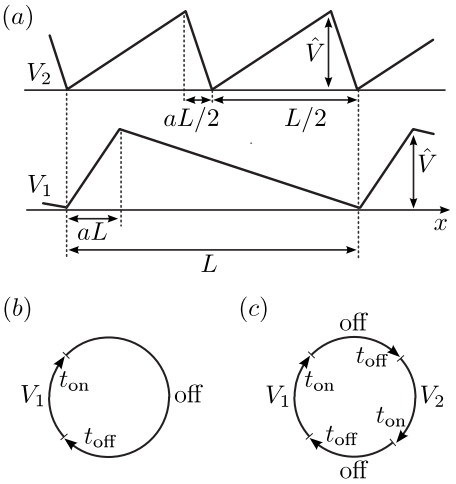

FIG. 2. (a) Spatial characteristics of the potentials used in the extended on-off ratchet. Short-periodic sawtooth potential V_2 (top), long-periodic sawtooth potential V_1 (bottom). (b) Cycle of a simple on-off ratchet. (c) Cycle of the extended on-off ratchet.

In order to change the direction of the mean displacement with another property than the asymmetry of the sawtooth potential, the on-off ratchet needs to be extended. For this purpose, we add a second sawtooth potential V_2 to the ratchet cycle. The cycle of our proposed extended on-off ratchet is schematically depicted in panel (c) of Fig. 2. As illustrated in panel (a) of Fig. 2, the second potential V_2 is characterized by half the spatial period $L/2$ and an inverse asymmetry parameter $(1-a)$. The two potentials are alternately activated with equal duration t_{on} and equal interjacent off times t_{off} so that the complete cycle lasts $T=2t_{\mathrm{off}}+2t_{\mathrm{on}}$. Due to their inverse asymmetries, the individual potentials induce drifts in opposite directions. In the extended on-off ratchet, both potentials are combined and the resulting direction of the mean displacement is no longer exclusively determined by the value of the asymmetry parameter a. In the following, we will define a set of four dimensionless parameters, which

fully characterizes the operation of the extended on-off ratchet. In particular, we will investigate which combinations of these parameters reverse the direction of the mean displacement.

In the extended on-off ratchet the motion of a Brownian particle with a friction coefficient γ is described by the Langevin equation

$$\gamma \frac{\partial}{\partial t} x = -\frac{\partial}{\partial x} V(x,t) + \xi(t), \tag{1}$$

where x denotes the position of the particle at the time t. As a function of t, the potential $V(x,t)$ changes cyclically between the two on states $V(x)=V_{1,2}(x)$ and the off state $V(x)=0$ [see the extended ratchet cycle in panel (c) of Fig. 2]. The random force $\xi(t)$ is unbiased so that $\langle \xi(t) \rangle = 0$ and its time-correlation function obeys the fluctuation-dissipation theorem

$$\langle \xi(t) \xi(t') \rangle = 2\gamma k_B T \delta(t-t'), \tag{2}$$

with $k_B T$ being the thermal energy. The description of the system in terms of the Langevin equation can be simplified by using rescaled variables. The spatial period L provides a length scale, whereas the typical time for the particle to cover the distance L by diffusion t_{diff} gives a time scale. The diffusion time t_{diff} is defined by

$$t_{\mathrm{diff}} = \frac{L^2}{D}, \tag{3}$$

with D being the diffusion constant. The Einstein relation $D=k_B T/\gamma$ relates the diffusion constant D to the friction constant γ. Another time scale is given by the drift time t_{drift}, which is the required time for the particle to drift the distance L under the constant force $\hat{V}/L$. With the drift velocity $v_{\mathrm{drift}}=\hat{V}/(\gamma L)$, the drift time takes the following form:

$$t_{\mathrm{drift}} = \frac{L}{v_{\mathrm{drift}}} = \frac{t_{\mathrm{diff}}}{\tilde{V}}, \tag{4}$$

where $\tilde{V}=\hat{V}/(k_B T)$ denotes the rescaled potential amplitude. The Langevin Eq. (1) and the correlation function [Eq. (2)] can now be expressed in reduced form

$$\frac{\partial}{\partial \tilde{t}} \tilde{x} = \tilde{V} f_a(\tilde{x},\tilde{t}) + \tilde{\xi}(\tilde{t}), \tag{5}$$

$$\langle \tilde{\xi}(\tilde{t}) \tilde{\xi}(\tilde{t}') \rangle = 2\tilde{\delta}(\tilde{t}-\tilde{t}'), \tag{6}$$

where we have introduced the rescaled position $\tilde{x}=x/L$, time $\tilde{t}=t/t_{\mathrm{diff}}$, random force $\tilde{\xi}(\tilde{t})=\xi(t)L/(k_B T)$, and δ function $\tilde{\delta}(\tilde{t})=t_{\mathrm{diff}}\delta(t)$. The function f_a describes the rescaled force exerted on the Brownian particle. When the potential is switched off, $f_a=0$ and Eq. (5) describes a particle freely diffusing in one dimension. When the potential V_i $(i=1,2)$ is switched on, $f_a=-c_i/a$ and $f_a=c_i/(1-a)$ on the long and short slopes of the potential, respectively. The constant c_i takes the values $c_1=1$ and $c_2=-2$. The rescaled potential amplitude $\tilde{V}$ is the Peclet number [26]. As shown by Eq. (4), it denotes the ratio of the times a particle needs to diffuse and drift a distance L. Therefore, at large Peclet numbers drift is dominant and Brownian diffusion during the application of the potential can be neglected. We will deal with this limit from here onwards.

We also rescale the periods of the ratchet cycle t_{on} and t_{off}. First, the off time t_{off} is rescaled with respect to the diffusion time t_{diff},

$$\tau_{\mathrm{off}} = \frac{t_{\mathrm{off}}}{t_{\mathrm{diff}}}. \tag{7}$$

For $\tau_{\mathrm{off}}<1$ Brownian particles are not able to cover a distance L by diffusion during the time t_{off}. Second, the on time t_{on} is rescaled with respect to the drift time t_{drift},

$$\tau_{\mathrm{on}} = \frac{t_{\mathrm{on}}}{t_{\mathrm{drift}}}. \tag{8}$$

For $\tau_{\mathrm{on}}>1$ all particles will drift into the minima of the potentials. In analogy with the rescaling of the time variable $\tilde{t}=t/t_{\mathrm{diff}}$, we also obtain $\tilde{t}_{\mathrm{on}}=\tau_{\mathrm{on}}/\tilde{V}$ and the period $\tilde{T}=2(\tau_{\mathrm{off}}+\tau_{\mathrm{on}}/\tilde{V})$ of one complete ratchet cycle.

In conclusion, the motion of a Brownian particle in the extended on-off ratchet depends on the rescaled off time τ_{off}, the rescaled on time τ_{on}, the asymmetry parameter a, and the Peclet number $\tilde{V}$. Our objective is to calculate the ensemble averaged displacement $\langle \Delta\tilde{x} \rangle$ per ratchet cycle, as a function of these four dimensionless variables, where the Peclet number $\tilde{V}$ will always be chosen much larger than one.

B. Brownian dynamics simulations

To solve the Langevin Eq. (5), we have performed Brownian dynamics simulations based on the standard Euler method, which is sufficient in view of the simplicity of the potential. Following this method, the position $\tilde{x}$ evolves during one time step $d\tilde{t}$ according to

$$\tilde{x}(\tilde{t}+d\tilde{t}) = \tilde{V} f_a(\tilde{x},\tilde{t}) d\tilde{t} + (2d\tilde{t})^{1/2} r(\tilde{t}). \tag{9}$$

Here, $(2d\tilde{t})^{1/2} r(\tilde{t})$ is the Wiener increment and $r(\tilde{t})$ is a random number from a distribution with zero mean $\langle r \rangle = 0$ and variance $\langle r^2 \rangle = 1$ [27]. To obtain sufficiently precise results, one million ratchet cycles were simulated for each combination of parameters.

The simulation results for the mean displacement $\langle \Delta\tilde{x} \rangle$ with $\tilde{V}=1000$ and $a=0.1$ and 0.3 are shown in panels (a) and (b) of Fig. 3, respectively. A common feature is that $\langle \Delta\tilde{x} \rangle$ becomes vanishingly small in the limit $\tau_{\mathrm{off}} \to 0$ and $\tau_{\mathrm{on}} \to 0$. Furthermore, for large values of τ_{off} and τ_{on} the mean displacement approaches a maximum value $\langle \Delta\tilde{x} \rangle_{\max}$. In Sec. III A, we will derive an analytical expression for $\langle \Delta\tilde{x} \rangle_{\max}$. In comparison with the simple on-off ratchet, the extended model exhibits some new features. In particular, the sign of $\langle \Delta\tilde{x} \rangle$ now depends on the values of τ_{off} and τ_{on}. Two regions are observed, in which $\langle \Delta\tilde{x} \rangle$ has opposite signs. The coordinates τ_{off}^* and τ_{on}^* of the curve which demarcates these two regions depend on the value of the asymmetry parameter a. In Sec. III A, we will treat the discrete regime with τ_{on}

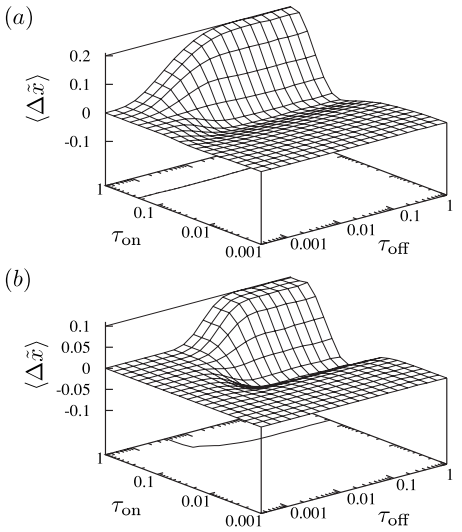

FIG. 3. (a) Mean displacements $\langle \Delta \tilde{x} \rangle$ obtained from a Brownian dynamics simulation with asymmetry $a=0.1$. (b) As in panel (a) but for $a=0.3$. The contour curves in the bottom planes correspond with $\langle \Delta \tilde{x} \rangle = 0$. These curves with coordinates τ_{off}^{*} and τ_{on}^{*} trace the points of the direction reversal of the mean displacement.

$> (1-a)^2$, i.e., when the particles always reach the minima of the potentials. As we will see, direction reversal only occurs for $a > 0.25$. A more pronounced direction reversal is achieved in the nondiscrete regime, with $\tau_{on} < (1-a)^2$ for sufficiently large values of τ_{off}. The latter direction reversal will be discussed in Sec. III B.

III. METHOD OF DISCRETE STEPS

To derive an analytic expression for the mean displacement $\langle \Delta \tilde{x} \rangle$ in the case of large Peclet numbers $\tilde{V}$, we apply the method of discrete steps [25]. As will be described in Sec. III A, this method is based on the assumption that the rescaled on time τ_{on} is sufficiently large so that a Brownian particle will always drift into a minimum when the sawtooth potentials are switched on. Hence, the trajectory of the particle can be mapped onto a sequence of effective steps between the locations of the potential minima. These steps occur with certain step probabilities. In Sec. III B, we successively extend the applicability of our method to smaller values of τ_{on} with the help of what we call the split-off approximation.

A. Discrete steps and their probabilities

For large Peclet numbers $\tilde{V}$, Brownian motion can be neglected once the potential is switched on. As a result, a particle drifts uniformly toward a minimum. For the longer slope of potential V_1, the drift velocity $v_{drift} = \hat{V}/[\gamma(1-a)L]$. Accordingly, the particle reaches the minimum for

$$t_{on} \geq \frac{(1-a)L}{v_{drift}} = (1-a)^2 t_{drift}, \tag{10}$$

irrespective of its position at the time the potential is switched on. With the definition of the rescaled on-time τ_{on}

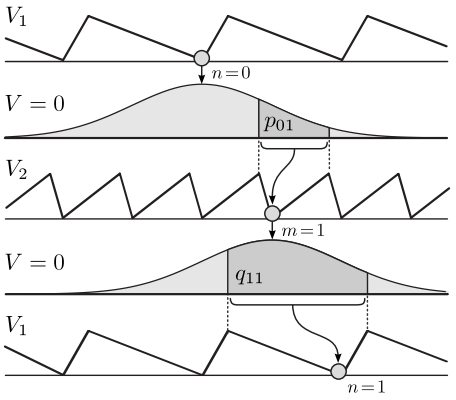

FIG. 4. Schematic illustration of a complete cycle of the extended on-off ratchet in the discrete limit. For one possible step combination $(n=0 \to m=1 \to n=1)$ the graphical interpretation of the corresponding step probabilities p_{01} and q_{11} is visualized.

[Eq. (8)], the latter condition can be expressed as

$$\tau_{on} \geq (1-a)^2. \tag{11}$$

Particles drifting under the influence of the shorter slope of potential V_1 as well as both slopes of potential V_2 also reach the minimum, provided Eq. (11) is satisfied. Accordingly, after each application of the potential, all particles are located at the minima of either V_1 or V_2. A single particle hence performs discrete steps along the x axis, provided its trajectory is sampled at the end of each on time. The minima of the potential V_1 are labeled with the integer n so that the corresponding positions are given by $\tilde{x}_n = n$. For the potential V_2, the minima are labeled with m and the positions are $\tilde{x}_m = m/2$ because V_2 has half the spatial periodicity.

Now, we consider the probability p_{nm} for a step performed by a single particle from the minimum n of V_1 to the minimum m of V_2, as illustrated in Fig. 4. When the potential is switched off the particle diffuses freely, starting from $\tilde{x}_S = n$. In our rescaled units, the probability density to reach the position $\tilde{x}$ at the end of the off time is given by the Gaussian distribution

$$g(\tilde{x}) = \frac{1}{\sqrt{4\pi\tau_{off}}} e^{-(\tilde{x}-\tilde{x}_S)^2/4\tau_{off}}. \tag{12}$$

Note that the width of this distribution is exclusively determined by the value of the rescaled off time τ_{off}. In order to drift to the minimum m of potential V_2 during the subsequent on time, the particle needs to diffuse into the interval $(m-a)/2 < \tilde{x} < (m+1-a)/2$ situated between the neighboring maxima of minimum m. Accordingly, the step probability is given by integrating $g(\tilde{x})$ so that

$$p_{nm} = \int_{(m-a)/2}^{(m+1-a)/2} \frac{d\tilde{x}}{\sqrt{4\pi\tau_{off}}} e^{-(\tilde{x}-n)^2/4\tau_{off}}. \tag{13}$$

In a similar way, we derive the probability q_{mn} for a step from the minimum m of V_2 to the minimum n of V_1. Now, the initial minimum is located at $\tilde{x}_S = m/2$ and the interval between the maxima around minimum n of V_1 is given by

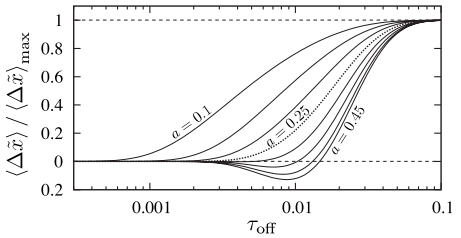

FIG. 5. Normalized mean displacement $\langle\Delta\tilde{x}\rangle/\langle\Delta\tilde{x}\rangle_{\max}$ in the extended on-off ratchet versus the rescaled off-time τ_{off}. The curves have been calculated in the discrete limit. From top to bottom, $a=0.1$, 0.15, 0.2, 0.25, 0.3, 0.5, 0.4, and 0.45. The dashed line with $a=0.25$ indicates the onset of direction reversal in an intermediate range of values for τ_{off}.

$(n-1+a)<\tilde{x}<(n+a)$. Hence, the step probability takes the form

$$q_{mn}=\int_{n-1+a}^{n+a}\frac{d\tilde{x}}{\sqrt{4\pi\tau_{\text{off}}}}e^{-(\tilde{x}-m/2)^2/4\tau_{\text{off}}}. \tag{14}$$

The mean displacement $\langle\Delta\tilde{x}\rangle$ is calculated for a complete ratchet cycle. Due to the spatial periodicity of the system, one can always place the initial minimum at $n=0$. By averaging over all possible step combinations, we arrive at

$$\langle\Delta\tilde{x}\rangle=\langle n\rangle=\sum_n\sum_m n\cdot p_{0m}q_{mn}. \tag{15}$$

Note that in the discrete limit the mean displacement $\langle\Delta\tilde{x}\rangle$ only depends on the values of the asymmetry parameter a and the rescaled off time τ_{off}.

We now discuss the limiting behavior of the mean displacement $\langle\Delta\tilde{x}\rangle$ for small and large values of τ_{off}. For small values of τ_{off}, the mean displacement approaches zero because the step probabilities to neighboring minima become vanishingly small. For large values of τ_{off}, the mean displacement takes its maximum value $\langle\Delta\tilde{x}\rangle_{\max}$. An algebraical expression for $\langle\Delta\tilde{x}\rangle_{\max}$ can be derived on the basis that the probability profile between two maxima becomes approximately homogeneous for large values of τ_{off}. The fractions of the particles experiencing the larger and shorter slopes of the potential V_1 are given by $(1-a)$ and a, respectively. The corresponding mean displacements of these fractions are $(1-a)/2$ and $-a/2$. The total mean displacement induced by potential V_1 is given by the weighed average of both fractions so that $\langle\Delta\tilde{x}_1\rangle=(1/2)-a$. The mean displacement induced by V_2 can be derived in the same way and yields $\langle\Delta\tilde{x}_2\rangle=-\langle\Delta\tilde{x}_1\rangle/2$. For the complete cycle, the mean displacement is given by the sum $\langle\Delta\tilde{x}\rangle=\langle\Delta\tilde{x}_1\rangle+\langle\Delta\tilde{x}_2\rangle$ so that

$$\langle\Delta\tilde{x}\rangle_{\max}=\lim_{\tau_{\text{off}}\to\infty}\langle\Delta\tilde{x}\rangle=\frac{1}{2}\left(\frac{1}{2}-a\right). \tag{16}$$

Note that this expression is only valid for sufficiently large values of the rescaled on time $\tau_{\text{on}}\geq(1-a)^2$.

We have obtained the mean displacement for a series of a values in the range $0.1<a<0.45$ by numerical evaluation of Eq. (15). The normalized values $\langle\Delta\tilde{x}\rangle/\langle\Delta\tilde{x}\rangle_{\max}$ with $\langle\Delta\tilde{x}\rangle_{\max}$ obtained from Eq. (16) are displayed in Fig. 5 as a function of the rescaled off time τ_{off}. For values of τ_{off} exceeding 0.1, the normalized mean displacement approaches unity. This confirms the predicted limiting behavior given by Eq. (16). For values of $a>0.25$, the normalized mean displacement becomes negative in an intermediate range of values of τ_{off}, i.e., the mean displacement changes its direction. The resulting minimum becomes more pronounced for larger values of a. Note that $\langle\Delta\tilde{x}\rangle_{\max}$ decreases linearly with a and reaches $\langle\Delta\tilde{x}\rangle_{\max}=0$ in the symmetric case with $a=0.5$. Accordingly, the minimum in the (un-normalized) mean displacement $\langle\Delta\tilde{x}\rangle$ vanishes in the limit $a=0.5$.

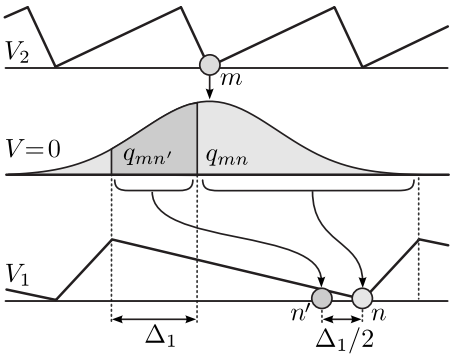

FIG. 6. Illustration of the split-off approximation on the longer slope of potential V_1. Particles corresponding with the dark gray colored part of the diffusion profile fail to reach the minimum n during the on time and will start the subsequent off time from the split-off point n'.

B. Split-off approximation

We now extend the method of discrete steps to values of τ_{on} smaller than $(1-a)^2$, i.e., not all particles will drift into a minimum of either potential V_1 or V_2 during the on time. For now, we restrict ourselves to the situation, where the particles on the longer slope of V_1 do not necessarily reach a minimum, but on the smaller slope and when potential V_2 is switched on they do. This situation corresponds to $(1-a)^2/4<\tau_{\text{on}}<(1-a)^2$.

We consider an ensemble of particles at a time right before the potential V_1 is switched on. Particles on the right-hand side of each maximum will not reach a minimum if they are located in a spatial region with a width Δ_1 as illustrated in Fig. 6. We will call Δ_1 the *split-off* parameter in the following. With the help of the drift velocity on the longer slope of V_1 and the length $(1-a)L$ of this slope, one is able to calculate the split-off parameter

$$\Delta_1=\max\left[0,(1-a)\left(1-\frac{\tau_{\text{on}}}{(1-a)^2}\right)\right]. \tag{17}$$

In order to apply the method of discrete steps, we assume that *all* particles in the region Δ_1 drift to a *single* split-off point n'. As illustrated in Fig. 6, this split-off point is located at a distance $-\Delta_1/2$ from the minimum with index n. The locations of the split-off points are hence given by $\tilde{x}_{n'}=n-\Delta_1/2$.

For $\tau_{\text{on}}<(1-a)^2/4$, we introduce additional split-off points on the longer slope of potential V_2. They are located at

$\tilde{x}_{m'}=(m+\Delta_2)/2$, where m indicates the minima of V_2. Particles in a certain region at the left-hand side of the maxima are not able to reach the minima of potential V_2. The width of this region Δ_2 is given by

$$\Delta_2 = \max\left[0, \frac{(1-a)}{2}\left(1 - \frac{\tau_{\rm on}}{\frac{1}{4}(1-a)^2}\right)\right]. \tag{18}$$

Obviously, our split-off approximation will result in a progressively worse estimation of the mean displacement for smaller values of $\tau_{\rm on}$ and, implicitly, larger values of Δ_1 and Δ_2.

We can derive an expression for the mean displacement in the same manner as in Sec. III A. Now we need to consider eight step probabilities. They are obtained by integrating over the corresponding sections of the diffusion profile. The split-off points are taken into account by a modification of the starting points $x_{\rm S}$ in Eq. (12) and the integration limits in Eqs. (13) and (14). Furthermore, in the expression for the mean displacement one has to introduce the respective probabilities P and P' for a particle to occupy either a minimum or the corresponding split-off point at the beginning of each cycle. Due to the spatial periodicity of the ratchet, these probabilities do not depend on the particular location n of the potential well. To determine $P(\tilde{t}_0+\tilde{T})$ and $P'(\tilde{t}_0+\tilde{T})$ from $P(\tilde{t}_0)$ and $P'(\tilde{t}_0)$ after one full ratchet cycle with period $\tilde{T}$, one has to consider all possible step combinations during such a cycle. Without loss of generality, all these step combinations are generated when one starts from the minimum at $n=0$ or the split-off point at $0'$. Therefore the probabilities P and P' evolve in time according to

$$P(\tilde{t}_0+\tilde{T}) = P(\tilde{t}_0)\sum_{m,n}(p_{0m}q_{mn} + p_{0m'}q_{m'n}) + P'(\tilde{t}_0)\sum_{m,n}(p_{0'm}q_{mn} + p_{0'm'}q_{m'n}), \tag{19}$$

$$P'(\tilde{t}_0+\tilde{T}) = P(\tilde{t}_0)\sum_{m,n}(p_{0m}q_{mn'} + p_{0m'}q_{m'n'}) + P'(\tilde{t}_0)\sum_{m,n}(p_{0'm}q_{mn'} + p_{0'm'}q_{m'n'}). \tag{20}$$

We are interested in the steady-state solution, $P(\tilde{t}_0+\tilde{T}) = P(\tilde{t}_0)$ and $P'(\tilde{t}_0+\tilde{T})=P'(\tilde{t}_0)$, which yields

$$\frac{P'}{P} = \frac{1-\sum_{m,n}(p_{0m}q_{mn}+p_{0m'}q_{m'n})}{\sum_{m,n}(p_{0'm}q_{mn}+p_{0'm'}q_{m'n})} = \frac{\sum_{m,n}(p_{0m}q_{mn'}+p_{0m'}q_{m'n'})}{1-\sum_{n,m}(p_{0'm}q_{mn'}+p_{0'm'}q_{m'n'})}. \tag{21}$$

Together with the normalization constraint $P+P'=1$, the probabilities P and P' are fully determined from either one of the conditions in Eq. (21). The mean displacement can now be derived by averaging over all possible step combinations (including the split-off points n' and m') and takes the following form:

$$\langle\Delta\tilde{x}\rangle = \sum_{n,m} n[(Pp_{0m}+P'p_{0'm})(q_{mn}+q_{mn'}) + (Pp_{0m'}+P'p_{0'm'})(q_{m'n}+q_{m'n'})]. \tag{22}$$

Here we approximate the step length by n, irrespective of whether the step starts or ends in a minimum or split-off point. Note that the mean displacement now depends on the parameters $\tau_{\rm on}$, $\tau_{\rm off}$, and a. In particular, the rescaled on time $\tau_{\rm on}$ enters through the values of the parameters Δ_1 and Δ_2 in the step probabilities. For $\tau_{\rm on}\geq(1-a)^2$, $\Delta_1=\Delta_2=0$ and Eq. (22) reduces to the corresponding Eq. (15) pertaining to discrete behavior.

We have obtained the mean displacement $\langle\Delta\tilde{x}\rangle$ according to the split-off approximation by numerical evaluation of Eq. (22) for $\tau_{\rm off}=1$ and $a=0.1$ and 0.3. The results are displayed in Fig. 7 as a function of the rescaled on time $\tau_{\rm on}$. For the sake of comparison, we have also included the corresponding values following from the Brownian dynamics simulation. The maximum value $\langle\Delta\tilde{x}\rangle_{\rm max}$, as given by Eq. (16), is recovered for $\tau_{\rm on}>(1-a)^2$. Note that the value $\tau_{\rm off}=1$ is sufficiently large for the application of Eq. (16) (see, e.g., Fig. 5). With decreasing values of $\tau_{\rm on}$, the mean displacement decreases and changes sign at a critical value of the rescaled on time $\tau_{\rm on}^*$. Irrespective of the value of the asymmetry parameter a, the prediction based on the split-off approximation is

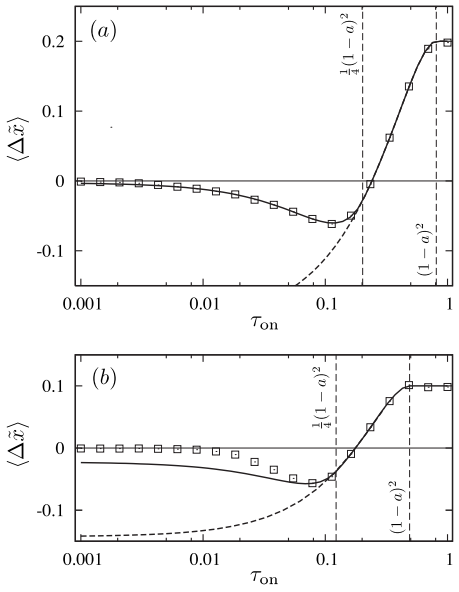

FIG. 7. (a) Mean displacement $\langle\Delta\tilde{x}\rangle$ in the extended on-off ratchet versus the rescaled on time $\tau_{\rm on}$ for a rescaled off time $\tau_{\rm off}=1.0$ and asymmetry parameter $a=0.1$. The solid curve refers to the results from the split-off approximation, whereas the symbols indicate the results from the Brownian dynamics simulations. The dashed curve refers to the results from the split-off approximation with $\Delta_2=0$ for all values of $\tau_{\rm on}$. The vertical dashed lines indicate the onset of the discrete regime at $\tau_{\rm on}=(1-a)^2$ and the threshold of the split-off approximation with $\Delta_2=0$ at $\tau_{\rm on}=(1-a)^2/4$. (b) As in panel (a), but for asymmetry parameter $a=0.3$.

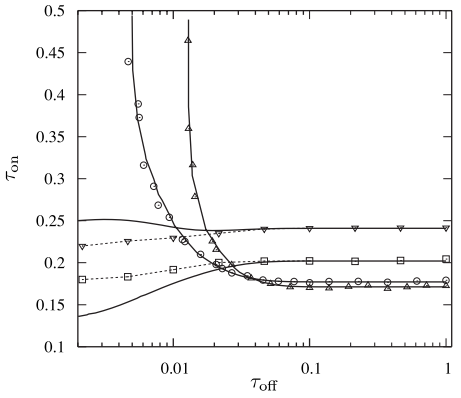

FIG. 8. Contour curves for $\langle \Delta\tilde{x} \rangle = 0$. These curves trace the points of direction reversal of the mean displacement with coordinates τ^*_{off} and τ^*_{on}. The symbols refer to Brownian dynamics simulation results with asymmetry parameters $a=0.1$ (∇), $a=0.2$ ($\square$), $a=0.3$ ($\circ$), and $a=0.4$ ($\triangle$). The solid curves represent the corresponding predictions based on the split-off approximation. The dashed curves serve as a guide to the eye. Notice that the latter predictions deviate from the simulation results for $a<0.3$ and $\tau^*_{off}<0.05$.

in perfect agreement with the results of the Brownian dynamics simulations in the range $(1-a)^2/4 < \tau_{on} < (1-a)^2$. The prediction even reproduces the behavior of $\langle \Delta\tilde{x} \rangle$ for smaller values of the rescaled on times (with deviations for $a=0.3$). In particular, for the present combination of parameters, the split-off approximation is sufficient to predict the point of direction reversal τ^*_{on}.

In order to compare the predictions based on the split-off approximation with the relevant results of the Brownian dynamics simulations for values of τ_{off} smaller than 1, we now consider the points of direction reversal of the mean displacement with coordinates τ^*_{off} and τ^*_{on} (i.e., those coordinates for which $\langle \Delta\tilde{x} \rangle = 0$). The corresponding contour curves following from the simulations as well as from the split-off approximation are displayed in Fig. 8 for some typical values of the asymmetry parameter a. The predictions of the points of direction reversal based on the split-off approximation are in perfect agreement with the simulation results for the larger values of the asymmetry parameter $a=0.3$ and 0.4, irrespective the value of the rescaled off time τ_{off}. In the case of smaller values of a, i.e., for $a=0.1$ and 0.2, the split-off approximation only gives accurate results for a sufficiently large value of $\tau_{off} > 0.05$. Furthermore, it should be noticed that for $\tau_{off} > 0.1$, the point of direction reversal of the mean displacement τ^*_{on} occurs at a constant but a dependent value, irrespective of the value of τ_{off}.

The split-off approximation also allows the calculation of the mean displacement $\langle \Delta\tilde{x} \rangle$ for large values of τ_{off} (in practice for $\tau_{off} > 0.1$). In the same way as for the derivation of Eq. (16), we obtain

$$\lim_{\tau_{off} \to \infty} \langle \Delta\tilde{x} \rangle = \frac{1}{2}\left(\frac{1}{2} - a\right) - \frac{1}{2}\Delta_1^2 + \Delta_2^2. \tag{23}$$

In the case of discrete behavior with $\Delta_1 = \Delta_2 = 0$, the latter expression correctly reduces to Eq. (16) for $\tau_{on} \geq (1-a)^2$.

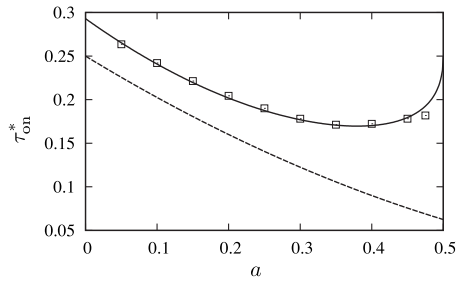

FIG. 9. Points of direction reversal of the mean displacement τ^*_{on} versus the asymmetry parameter a. The solid curve represents the prediction based on the split-off approximation in the limit of large values of τ_{off}. The symbols refer to the corresponding results from the Brownian dynamics simulations. The dashed curve demarcates the region $\tau_{on} > (1-a)^2/4$, where the split-off approximation with $\Delta_2 = 0$ applies.

Furthermore, Eq. (23) allows the derivation of an expression for the point of direction reversal τ^*_{on}. We first solve $\lim_{\tau_{off} \to \infty} \langle \Delta\tilde{x} \rangle = 0$ for the split-off parameter Δ_1 with $\Delta_2 = 0$ and use Δ_1 in Eq. (17) to calculate the rescaled on time

$$\tau^*_{on} = (1-a)^2 \left[1 - \left(\frac{\frac{1}{2} - a}{(1-a)^2} \right)^{1/2} \right]. \tag{24}$$

Note that in the limit of $\tau_{off} \to \infty$, the value of τ^*_{on} only depends on the asymmetry parameter a. The predicted values for τ^*_{on} are displayed in Fig. 9 as a function of the asymmetry parameter a. Excellent agreement with the corresponding results from the Brownian dynamics simulations is observed for $a < 0.45$. Furthermore, we note that the predicted values for τ^*_{on} fall within the region $\tau_{on} > (1-a)^2/4$, where the split-off approximation applies for $\Delta_2 = 0$. Our *a priori* choice of $\Delta_2 = 0$ is hence justified.

In principle, the split-off approximation can be carried to higher levels by including split-off points on all slopes. We have however refrained from doing so because the mathematical expressions become rather involved and there is not much gain in physical insight. Furthermore, very small values of τ_{on} are of little interest from a practical point of view because the corresponding mean displacements are vanishingly small.

IV. PARTICLE SEPARATION

A novel feature of the extended on-off ratchet is that the magnitude and the direction of the mean displacement can be varied by adjusting the parameters τ_{off} and τ_{on}. In the following we discuss how this feature can be used to improve the separation in microfluidic sieve devices. In the introduction we already proposed two designs for such devices (see Fig. 1). Here, our objective is to translate the parameters of the extended on-off ratchet model to real design parameters. In particular, we will explore how we can experimentally control the magnitude and direction of the mean displacement of the particles induced by the sieve devices.

In the classical sieve as well as in our proposed designs, the rectification of the Brownian motion is based on the in-

teraction between electrophoretically driven particles and asymmetrically shaped obstacles. Before we discuss particle separation, we need to define the time scales for diffusion and drift. For a particle with an electrophoretic mobility μ_E in an electric field with strength E, the electrophoretic velocity is given by $v_E=\mu_E E$. In contact with an obstacle, the direction of the velocity changes and acquires a component $v_{E,x}$ in the direction perpendicular to the electric field. Assuming that the face of the obstacle is tilted by the angle θ from the direction of the electric field, the transverse component amounts to $v_{E,x}(\theta)=v_E \sin\theta\cos\theta$. We now introduce the largest possible tilt angle $\theta_{\max}=\mathrm{atan}(L/h)$ for obstacles with lateral extension L and height h [see panel (b) of Fig. 1] and define the characteristic drift time $t_{\mathrm{drift}}=L/v_{E,x}(\theta_{\max})$ in full analogy to Eq. (4). The diffusion time $t_{\mathrm{diff}}=L^2/D$ remains the same and the Peclet number reads $t_{\mathrm{diff}}/t_{\mathrm{drift}}=Lv_{E,x}(\theta_{\max})/D$. Accordingly, it can be tuned by adjusting the strength of the electric field.

In the classical sieve device, charged particles are driven through rows of identical obstacles with the help of an externally applied electric field. Between the rows of obstacles, particles freely diffuse in the direction perpendicular to the applied field. The particles can only pass the rows through gaps between the obstacles. Hence, the particles are displaced in the direction perpendicular to the electric field each time they pass a row. Due to the asymmetric shape of the obstacles, the mean displacement has a nonzero value. As a consequence, the direction of the net flow of the particles is tilted from the direction of the electric field. If the associated tilt angle depends on particle-specific properties, different types of particles will move in different directions. For sufficiently large values of the Peclet number, the mean displacement and hence the tilt angle can be calculated by means of step probabilities between the gaps of adjacent rows of obstacles [5,6,9].

For large values of τ_{on}, the extended on-off ratchet model is in the regime of discrete steps described in Sec. III A. This case is directly implemented by the modified classical sieve of panel (a) in Fig. 1, where every second row of obstacles is replaced by a row of obstacles with half the spatial periodicity and inverse asymmetry. The shapes of the obstacles in subsequent rows reflect the spatial dependencies of the potentials V_1 and V_2 [see panel (a) of Fig. 2]. We have also chosen the shape of the obstacles to be invariant under reversal of the direction of the electric field. The off time of the ratchet is determined by the time the particles need to cross the distance d between the rows under the influence of the electric field and is given by $t_{\mathrm{off}}=d/v_E$. Accordingly, the value of t_{off} and hence the rescaled off time,

$$\tau_{\mathrm{off}}=\frac{dD}{\mu_E E L^2} \tag{25}$$

can experimentally be tuned by adjusting the strength of the electric field E. Suppose that a suspension contains two types of particles A and B with different values for D/μ_E [5]. In order to separate these particles in a sieve with a rescaled off time for direction reversal τ_{off}^*, the rescaled off times pertaining to the two types of particles have to be tuned such that $\tau_{\mathrm{off,A}}>\tau_{\mathrm{off}}^*>\tau_{\mathrm{off,B}}$. As a consequence, the net flows of both types of particles are tilted in opposite directions from the direction of the electric field. The methods presented in Sec. III A can be used to determine the value of τ_{off}^* for a device specific value of the asymmetry parameter a. Note that for large values of τ_{on}, the value of a has to exceed 0.25 to observe direction reversal of the mean displacement (see Fig. 5). According to Ref. [9], the sieve device can be operated in combination with a periodic reversal of the direction of the electric field. In this case, only a few rows of obstacles are necessary and the device can be downsized in y direction without reducing the resolution of the separation process. Note that our extension of the classical sieve device leads to a separation of both types of particles even in the case of a nonlocalized injection of the particles.

In the classical sieve and its modification as described above, all particles eventually have to pass through the gaps in the rows of obstacles. Accordingly, this design does not allow the implementation of the nondiscrete regime, which we treated by the split-off approximation in Sec. III B. We therefore propose an alternative design illustrated in panel (b) of Fig. 1, where the sawtooth-shaped obstacles now line the two opposing walls of a channel. The profiles of the walls mimic the spatial dependencies of potentials V_1 and V_2. Rather than driving the particles through subsequent rows of obstacles, the particles are driven back and forth between the two opposing walls of the channel with the help of a periodically inverted electric field. Note that the electric field is applied perpendicular to the direction of the channel. We define the time periods T_+ and T_- to indicate the periods over which the electric field points up and downwards, i.e., in the positive and negative y direction, respectively.

For a simplified analysis of the channel device, we set $T_+ \gg d/v_E$. As a consequence, the particles always reach the upper wall of the channel, meaning that they completely drift into the grooves of the sawtooth profile. The performance of the proposed device now depends on the period T_- of the pulsed electric field, the distance between the rows d, the height of the sawtooth profiles h, and the electrophoretic velocity of the particles v_E. Four different regimes can be identified. In the first regime with $T_-<h/v_E$, the particles are trapped within one spatial period of the upper row of obstacles and no mean displacement occurs. Note that the limits of the four regimes, which we present here, are approximate values because of the Brownian motion in y direction. In the second regime with $h/v_E<T_-<(d+h)/v_E$, the particles only interact with the upper row of obstacles. Hence the channel functions as a simple on-off ratchet. The value of the induced mean displacement is determined by the off time $t_{\mathrm{off}}\approx 2(T_- - h/v_E)$ and is negative due to the inverse asymmetry of the profile. For sufficiently large values of t_{off}, the displacement is given by $\langle\Delta\tilde{x}\rangle=-(1/2-a)/2$ [25]. In the third regime with $(d+h)/v_E<T_-<(d+2h)/v_E$, the particles interact with both rows of obstacles, however, they will not always drift into the grooves of the sawtooth profile of the lower wall before their electrophoretic direction is reversed by switching the electric field. In this regime, the mean displacement can approximately be described by the split-off approximation of the extended on-off ratchet. The off time is determined by the time the particles need to cross the distance d between the upper and lower rows. Hence, the res-

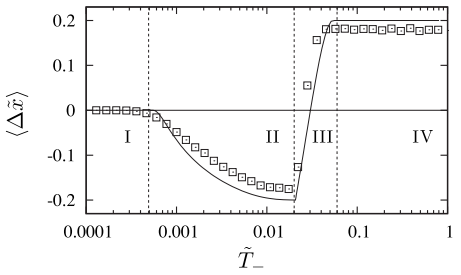

FIG. 10. Mean displacement $\langle \Delta \tilde{x} \rangle$ of a particle in a channel device as a function of the reduced time period $\tilde{T}_-$ in units of t_{diff}. The geometry of the channel is defined by the asymmetry parameter $a=0.1$ and the reduced lengths $\tilde{h}=0.1$ and $\tilde{d}=4$ in units of L. The symbols refer to results from two-dimensional Brownian dynamics simulations. The solid line refers, respectively, to predictions from the conventional and the extended on-off ratchet model. The vertical lines demarcate the different operational regimes of the channel device, as discussed in the text.

caled off time is given by Eq. (25). The time during which the particles are in contact with the lower row of obstacles determines the on time $t_{\mathrm{on}} \approx T_- - (d+h)/v_E$. Its rescaled value

$$\tau_{\mathrm{on}} = \sin\,\theta_{\mathrm{max}} \cos\,\theta_{\mathrm{max}} \frac{\mu_E E T_- - (d+h)}{L} \tag{26}$$

can be tuned by adjusting the product ET_- properly. Note that in this regime changes in T_- only affect τ_{on} whereas τ_{off} remains constant. In the fourth regime with $T_- > (d+2h)/v_E$ the particles always reach the walls of the channel before their electrophoretic velocity changes direction. In this regime, the channel is equivalent to our sieve design proposed above.

The equations derived under the split-off approximation require minor modification in order to describe the mean displacement in the third regime. For given values of h and L, we have already defined the maximum tilt angle $\theta_{\mathrm{max}} = \mathrm{atan}(L/h)$. It occurs for asymmetry parameter $a=0$. For nonzero a we define the tilt angle of the longest slope of the two obstacles, $\theta_a < \theta_{\mathrm{max}}$. Compared to the drift velocity induced by the sawtooth potential in Sec. II, the electrophoretic velocity $v_{E,x}(\theta_a)$ exhibits a different dependence on the asymmetry parameter a and the adjusted split-off parameter Δ_1 now reads

$$\Delta_1 = (1-a) - \tau_{\mathrm{on}} \frac{v_{E,x}(\theta_a)}{v_{E,x}(\theta_{\mathrm{max}})}. \tag{27}$$

Due to our choice for T_+, the second split-off parameter $\Delta_2 = 0$ is zero.

We performed two-dimensional Brownian dynamics simulations of a particle in the proposed channel device. The interaction between the particle and a wall was modeled with a short-ranged repulsive potential V_{wall}. For a reduced particle-wall distance $\tilde{r}$ in units of L, the potential is given by $V_{\mathrm{wall}}(\tilde{r})/k_{\mathrm{B}}T = (\tilde{r}/b)^{-12}$ with $b = 1.25 \times 10^{-3}$. The asymmetry parameter and the reduced lengths of the channel geometry were set to $a=0.1$, $\tilde{h}=0.1$, and $\tilde{d}=4$, and the Peclet number was chosen as $t_{\mathrm{diff}}/t_{\mathrm{drift}} \approx 20$. Figure 10 shows the mean displacement $\langle \Delta \tilde{x} \rangle$ as a function of the reduced period $\tilde{T}_-$ in units of t_{diff}. We have demarcated the four regimes with increasing $\tilde{T}_-$ as discussed above. In each regime, the results of the simulations are compared to the predictions of the corresponding model, i.e., zero displacement in regime I, simple on-off ratchet in regime II, extended on-off ratchet with nondiscrete behavior in regime III, and extended on-off ratchet with discrete behavior in regime IV, respectively. In all four regimes the predictions are in good agreement with the results from the simulations. Most of all, the reversal of the drift direction in the third regime is correctly predicted by the extended on-off ratchet within the split-off approximation. Deviations between the extended ratchet model and the simulation data are due to four main reasons. First, the one-dimensional model neglects diffusion of the particle in y direction. Second, the model does not take into account that on and off times depend on the exact position of the particle at times when the electric field is reversed. Third, the model assumes that the particles can diffuse freely in x direction even in the vicinity of the obstacles. Fourth, the simulation was performed for Peclet number $t_{\mathrm{diff}}/t_{\mathrm{drift}} \approx 20$, whereas the model refers to $t_{\mathrm{diff}}/t_{\mathrm{drift}} \gg 1$. Although the extended ratchet model is a simplification of the actual particle dynamics in the channel geometry, it offers a fairly good prediction of the mean displacements.

Now we assume that particles of types A and B with different values for μ_E are present in the channel. The suspension should be sufficiently diluted so that particle interactions can be neglected. To each particle type belongs a curve similar to the one plotted in Fig. 10. However, the limits of the different regimes depend on the properties of the particles. Particles A and B are effectively separated when they move in opposite directions along the channel. This means one has to identify values for $\tilde{T}_-$, where the signs of the mean displacements $\langle \Delta \tilde{x} \rangle$ of particles A and B differ. The involved parameters can be used to tune the system appropriately.

V. CONCLUSIONS

We have introduced an extension of the standard on-off ratchet by including a second asymmetric sawtooth potential with half the periodicity and inverse asymmetry in the ratchet cycle. As a result of this additional potential, Brownian particles exhibit direction reversal of their mean displacement. Analysis of the Langevin equation reveals that the motion of the particles and, hence, their mean displacement depend on four dimensionless parameters: the Peclet number, the asymmetry of the potentials, and the rescaled on and off times. We have derived analytical expressions for the mean displacement, based on the method of discrete steps and the split-off approximation. We show that these expressions are valid in relevant regions of the parameter space and that they can be used to predict locations in parameter space where direction reversal occurs. We have concentrated on the ratio 1:2 for the periods of the two sawtooth potentials. However, the formalism presented here can also be applied to other ratios, albeit some expressions will require modifications due to changes in the symmetry of the system.

We have demonstrated that our ratchet model offers opportunities for the separation of particles in microfluidic devices. In particular, we have shown that the application of direction reversal can overcome the major drawbacks of the classical sieve designs. Therefore, we have proposed two different designs with significantly reduced system sizes without sacrificing the resolution of the separation process. Exploiting direction reversal in the non-discrete ratchet regime allows a reduction in the device to a *single* channel. Furthermore in both designs nonlocalized injection is possible, which leads to an increased throughput. We demonstrate that the model of the extended on-off ratchet is able to describe the dynamics of a single particle in the proposed sieve devices. However, one should bear in mind that the model is a simplification. Many-particle effects due to electrostatic and hydrodynamic interactions among the particles are not included. Hydrodynamic interactions between the particles and the obstacles are also neglected. However, the interplay between Brownian motion and hydrodynamic wall effects is not expected to impair particle separation [8]. Furthermore, we have assumed a homogeneous electric field that is not disturbed by the presence of the obstacles. For a classical sieve, it has been shown that the efficiency of the device will be reduced if the electric field cannot penetrate the obstacles [28]. Further numerical studies including collective effects due to electrostatic and hydrodynamic interactions are in progress. It should be noted, however, that the impact of collective phenomena can always be made vanishingly small by sufficiently diluting the suspension.

[1] T. M. Squires and S. R. Quake, Rev. Mod. Phys. **77**, 977 (2005).
[2] N. Pamme, Lab Chip **7**, 1644 (2007).
[3] L. R. Huang, E. C. Cox, R. H. Austin, and J. C. Sturm, Anal. Chem. **75**, 6963 (2003).
[4] C. F. Chou, O. B. Bakajin, S. W. Turner, T. A. J. Duke, S. S. Chan, E. C. Cox, H. Craighead, and R. H. Austin, Proc. Natl. Acad. Sci. U.S.A. **96**, 13762 (1999).
[5] T. A. J. Duke and R. H. Austin, Phys. Rev. Lett. **80**, 1552 (1998).
[6] D. Ertaş, Phys. Rev. Lett. **80**, 1548 (1998).
[7] K. D. Dorfman and H. Brenner, J. Colloid Interface Sci. **238**, 390 (2001).
[8] K. D. Dorfman and H. Brenner, Phys. Rev. E **65**, 052103 (2002).
[9] I. Derenyi and R. D. Astumian, Phys. Rev. E **58**, 7781 (1998).
[10] P. Reimann, Phys. Rep. **361**, 57 (2002).
[11] S.-H. Lee, K. Ladavac, M. Polin, and D. G. Grier, Phys. Rev. Lett. **94**, 110601 (2005).
[12] Y. D. Chen, B. Yan, and R. Miura, Phys. Rev. E **60**, 3771 (1999).
[13] M. Bier, Phys. Lett. A **211**, 12 (1996).
[14] R. Kanada and K. Sasaki, J. Phys. Soc. Jpn. **68**, 3759 (1999).
[15] J. Rousselet, L. Salome, A. Ajdari, and J. Prost, Nature (London) **370**, 446 (1994).
[16] L. Gorre-Talini, S. Jeanjean, and P. Silberzan, Phys. Rev. E **56**, 2025 (1997).
[17] L. P. Faucheux, L. S. Bourdieu, P. D. Kaplan, and A. J. Libchaber, Phys. Rev. Lett. **74**, 1504 (1995).
[18] S. Matthias and F. Müller, Nature (London) **424**, 53 (2003).
[19] J.-F. Chauwin, A. Ajdari, and J. Prost, Europhys. Lett. **32**, 373 (1995).
[20] M. Kostur and J. Luczka, Phys. Rev. E **63**, 021101 (2001).
[21] P. Reimann and M. Evstigneev, EPL **78**, 50004 (2007).
[22] R. Eichhorn, P. Reimann, and P. Hänggi, Physica A **325**, 101 (2003).
[23] R. Eichhorn, A. Ros, J. Regtmeier, T. Tu Duong, P. Reimann, and D. Anselmetti, Eur. Phys. J. Spec. Top. **143**, 159 (2007).
[24] A. Ros, R. Eichhorn, J. Regtmeier, T. Tu Duong, P. Reimann, and D. Anselmetti, Nature (London) **436**, 928 (2005).
[25] A. Ajdari and J. Prost, C. R. Acad. Sci., Ser. II: Mec., Phys., Chim., Sci. Terre Univers **315**, 1635 (1992).
[26] J. Dhont, *An Introduction to Dynamics of Colloids* (Elsevier, Amsterdam, 1996).
[27] P. E. Kloeden and E. Platen, *Numerical Solution of Stochastic Differential Equations* (Springer, Berlin, Heidelberg, 1992).
[28] Z. Li and G. Drazer, Phys. Rev. Lett. **98**, 050602 (2007).